OPEN

Molecular Psychiatry (2015) 20, 361–368

www.nature.com/mp

ORIGINAL ARTICLE

Phenotypic differences in hiPSC NPCs derived from patients with schizophrenia

K Brennand[1,2,3,11], JN Savas[4,12], Y Kim[3,12], N Tran[1,3,12], A Simone[3,12], K Hashimoto-Torii[5,6], KG Beaumont[7,8], HJ Kim[3], A Topol[1], I Ladran[1,3], M Abdelrahim[1], B Matikainen-Ankney[2], S-h Chao[9], M Mrksich[7,8], P Rakic[5], G Fang[10], B Zhang[10], JR Yates III[4] and FH Gage[3]

Consistent with recent reports indicating that neurons differentiated *in vitro* from human-induced pluripotent stem cells (hiPSCs) are immature relative to those in the human brain, gene expression comparisons of our hiPSC-derived neurons to the Allen BrainSpan Atlas indicate that they most resemble fetal brain tissue. This finding suggests that, rather than modeling the late features of schizophrenia (SZ), hiPSC-based models may be better suited for the study of disease predisposition. We now report that a significant fraction of the gene signature of SZ hiPSC-derived neurons is conserved in SZ hiPSC neural progenitor cells (NPCs). We used two independent discovery-based approaches—microarray gene expression and stable isotope labeling by amino acids in cell culture (SILAC) quantitative proteomic mass spectrometry analyses—to identify cellular phenotypes in SZ hiPSC NPCs from four SZ patients. From our findings that SZ hiPSC NPCs show abnormal gene expression and protein levels related to cytoskeletal remodeling and oxidative stress, we predicted, and subsequently observed, aberrant migration and increased oxidative stress in SZ hiPSC NPCs. These reproducible NPC phenotypes were identified through scalable assays that can be applied to expanded cohorts of SZ patients, making them a potentially valuable tool with which to study the developmental mechanisms contributing to SZ.

Molecular Psychiatry (2015) **20,** 361–368; doi:10.1038/mp.2014.22; published online 1 April 2014

INTRODUCTION

Though the characteristic symptoms of schizophrenia (SZ) generally appear late in adolescence, it is thought to be a neurodevelopmental condition[1] that is often predated by a prodromal period that can appear in childhood.[2] Although postmortem studies have identified defects in neurons, such as reduced neuronal size and spine density in the prefrontal cortex and hippocampus,[3] these findings represent disease end points and reveal little about disease predisposition or initiation. Because damaging *de novo* mutations in persons with SZ converge in a network of genes co-expressed in the prefrontal cortex during fetal development,[4] one prevailing hypothesis is that disruptions in fetal prefrontal cortical development underlie SZ.

Human cell-based models of many brain diseases have been established by reprogramming patient somatic cells into human-induced pluripotent stem cells (hiPSCs). Although hiPSC neurons are electrophysiologically active, gene expression patterns indicate that they are immature relative to those in the human brain.[5,6] hiPSCs can be differentiated into cortical pyramidal[7] and interneuron fate,[5,8] but these neurons require months to fully mature *in vitro* and generally lack myelination.[9,10] Conversely, neural progenitor cells (NPCs) are a highly replicative neural population capable of rapidly initiating neuronal differentiation; they are easily assayed and particularly well suited to scalability. Given these advantages, we hoped to identify cellular phenotypes in SZ hiPSC NPCs that might be suitable for screening larger cohorts of SZ patients.

METHODS

For more detailed information, please refer to 'Extended Experimental Procedures' in Supplementary Information.

Description of SZ patients

All patient and control NPCs were differentiated from hiPSCs reprogrammed from fibroblasts obtained from the Coriell Cell Repository (Camden, NJ, USA) or American Type Culture Collection (Manassas, VA, USA). In total, NPCs from four patients and six controls were compared.

NPC culture

hiPSC forebrain NPCs were derived as described previously.[11] Forebrain NPCs were maintained at high density, grown on either Matrigel or poly-ornithine/laminin-coated plates in NPC media (Dulbecco's Modified Eagle Medium/Ham's F12 Nutrient Mixture, 1x N2, 1x B27-RA (Life Technologies, Carlsbad, CA, USA)), 1 μg ml^{-1} laminin (Life Technologies) and 20 ng ml^{-1} Fibroblast Growth Factor 2 (Life Technologies) and split ~1:3–1:4 every week with Accutase (Millipore, Billerica, MA, USA).

[1]Department of Psychiatry, Icahn School of Medicine at Mount Sinai, New York, NY, USA; [2]Department of Neuroscience, Icahn School of Medicine at Mount Sinai, New York, NY, USA; [3]Salk Institute for Biological Studies, Laboratory of Genetics, La Jolla, CA, USA; [4]Department of Chemical Physiology, The Scripps Research Institute, La Jolla, CA, USA; [5]Department of Neurobiology and Kavli Institute for Neuroscience, Yale University School of Medicine, New Haven, CT, USA; [6]Center for Neuroscience Research, Children's National Medical Center, Washington DC, USA; [7]Departments of Chemistry, Northwestern University, Evanston, IL, USA; [8]Department of Biomedical Engineering, Northwestern University, Evanston, IL, USA; [9]Center for Biosignatures Discovery Automation, Biodesign Institute, Arizona State University Tempe, Arizona, AZ, USA and [10]Department of Genetics and Genomic Sciences, Icahn School of Medicine at Mount Sinai, New York, NY, USA. Correspondence: Dr KJ Brennand or Professor FH Gage, Salk Institute for Biological Studies, Laboratory of Genetics, 10010 North Torrey Pines Road, La Jolla, CA 10029, USA.
E-mail: kristen.brennand@mssm.edu or gage@salk.edu
[11]Current address: Department of Psychiatry, Icahn School of Medicine at Mount Sinai, 1425 Madison Avenue, New York, NY 10029, USA.
[12]These authors contributed equally to this work.
Received 27 June 2013; revised 30 January 2014; accepted 3 February 2014; published online 1 April 2014

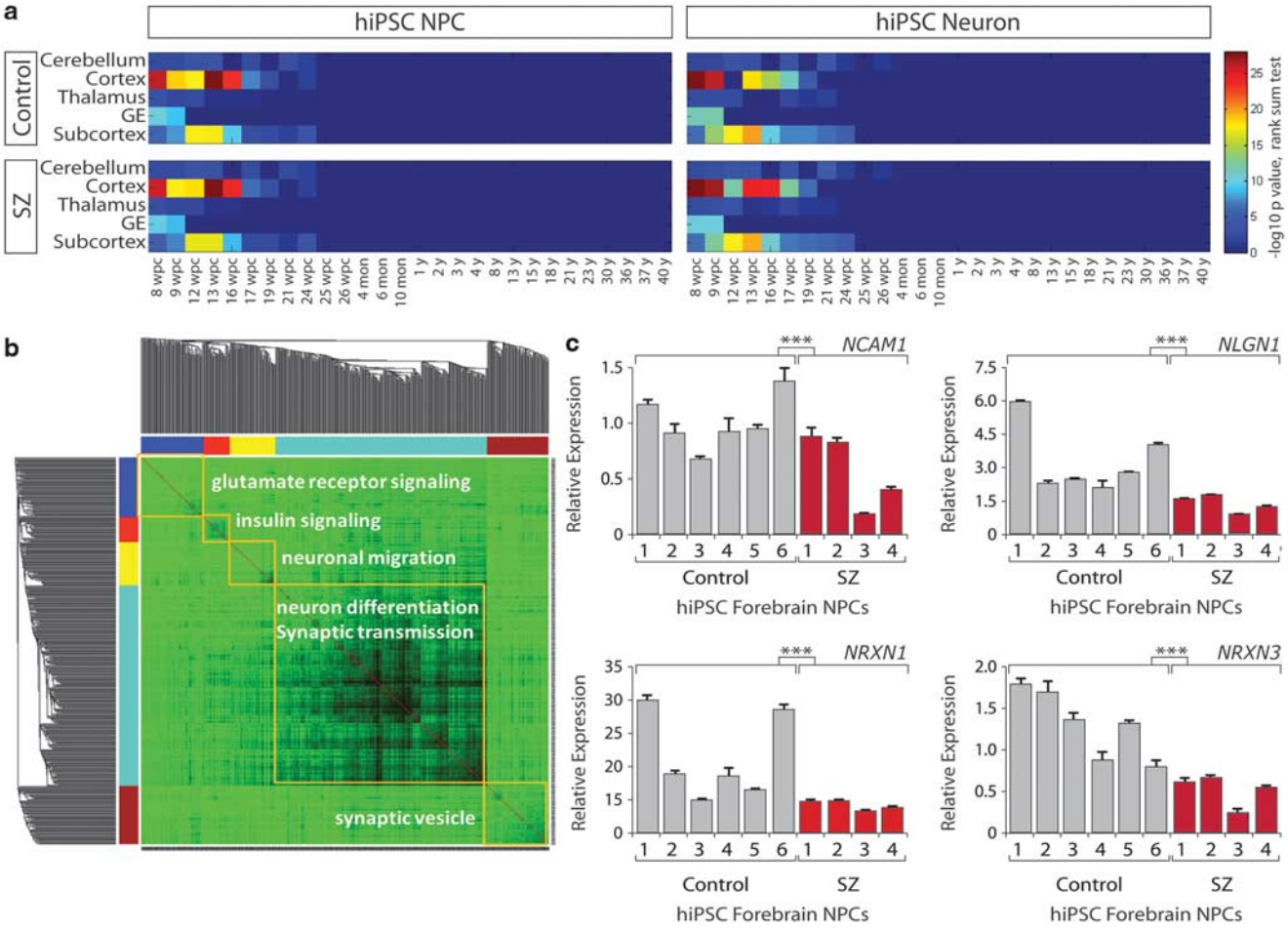

Figure 1. Gene expression of control and schizophrenia (SZ) human-induced pluripotent stem cell (hiPSC) neural progenitor cells (NPCs) and 6-week-old neurons most resembles human first trimester forebrain tissue. (**a**) Heatmaps produced by Wilcoxon's rank-sum comparisons of control and SZ hiPSC forebrain NPC and 6-week-old neuron microarray gene expression relative to the Allen BrainSpan Atlas. (**b**) WGCNA (weighted gene co-expression network analysis) of the SZ NPC gene signature identified five modules. (**c**) Quantitative PCR validation of the altered expression of the adhesion genes *NCAM1, NLGN1, NRXN1* and *NRXN3* in hiPSC forebrain NPCs from six controls and four SZ patients. Error bars are s.e.m., $^{***}P < 0.001$. See also Supplementary Figures 1–6.

Gene expression analysis

Cross-platform comparisons of our hiPSC microarray and the AllenBrain Atlas microarrays were done by (1) ranking absolute gene expression for each microarray using Partek, (2) assigning a rank difference value for each gene using a MATLAB script, and (3) calculating Spearman Rank Correlation Coefficients for each microarray comparison in Microsoft Excel. Wilcoxon's rank-sum test was assessed if a category of interest (spatial, temporal or combined) had significantly higher Spearman correlations than the background of all pairwise correlations. No hard cutoffs of 'best matches' were used. Methods for using weighted gene co-expression network analysis (WGCNA) to identify modules composed of highly co-expressed genes were previously published.[12]

SILAC analysis

To label hiPSC NPCs with stable isotope amino acids, cells were cultured in NPC media for 10 days (~ 4–5 population doublings) with or without heavy isotope ($^{13}C^{15}N$)-enriched arginine and lysine (Cambridge Isotopes); heavy labeled cells were cultured in medium depleted of light arginine and lysine (Life Technologies) before harvest. Protein identification, quantification and analysis were done with Integrated Proteomics Pipeline—IP2 (Integrated Proteomics Applications, www.integratedproteomics.com/) using Pro-LuCID, DTASelect2, Census and QuantCompare.[13]

Cellular phenotype assays

Neurosphere migration assay. NPCs were dissociated with Accutase and then cultured for 72 h in non-adherent plates to generate neurospheres. Neurospheres were manually picked and cultured in Matrigel matrix (0.5 mg Matrigel was plated in cold NPC media to a 96-well plate 1 h before neurosphere plating; following neurosphere picking, additional Matrigel was added, again as 0.5 mg in cold NPC media per 96-well plate). Average migration from each neurosphere was measured using NIH Image J.

NPC oxidative stress assays. OxyBlot assay (Millipore) was performed according to the manufacturer's instructions. Mitochondrial membrane potential (MMP) was assayed by fluorescence-activated cell sorting (FACS) analysis following incubation with the JC-1 lipophilic cationic dye (Life Technologies). Geometric median intensity was calculated using FlowJo software (TreeStar, Ashland, OR, USA).

Statistical analysis

For phenotypic and quantitative PCR (qPCR) analysis, statistical analysis was performed using JMP (Carey, NC, USA). Box-Cox transformation of raw data was performed to correct non-normal distribution of the data and residuals. Improvements were assessed by Shapiro–Wilk W-test of the transformed data and residuals. Means were compared within diagnosis by

one-way analysis using both Student's *t*-test and Tukey-Kramer honest significant difference test. Nested analysis of values for individual patients was performed using standard least squares analysis, comparing means for all pairs using Student's *t*-test for specific pairs and Tukey-Kramer honest significant difference test for multiple comparisons. In all figures, error bars represent s.e.m., $*P < 0.05$, $**P < 0.01$, $***P < 0.001$.

RESULTS

Characterization of control and SZ hiPSC NPCs

Figure 1 shows that gene expression profiles of hiPSC-derived neural cells most closely recapitulate those of the fetal forebrain. We compared hiPSC forebrain NPC and 6-week-old neuron microarray gene expression profiles to the Allen BrainSpan: Atlas of the Developing Human Brain (http://www.brainspan.org) using Spearman Rank Correlation analysis, and found that control and SZ hiPSC forebrain NPCs and 6-week-old neurons shared the most similarity with first trimester fetal brain tissue (Figure 1a and Supplementary Figure 1). Heatmaps generated through a Wilcoxon's rank-sum test revealed that the earliest time points of brain tissue (8–16 weeks post conception for hiPSC NPCs, 8–24 weeks post conception for hiPSC 6-week-old neurons) were consistently enriched with high significance, particularly in the cortical and subcortical forebrains and the ganglionic eminence. Control and SZ hiPSC NPCs and 6-week-old neurons shared highly similar spatial/temporal profiles relative to the Allen BrainSpan Atlas (Figure 1a); the correlation between control and SZ spatio-temporal similarity relative to the Allen Brain Atlas (– log10 p rank-sum test) for the NPCs was 0.9993 ($P < 1.4e{-}48$), whereas for the 6-week-old neurons it was 0.9670 ($P < 9.1e{-}19$). Each patient and control showed very similar spatial and temporal identity relative to the human brain, with very minimal inter-individual variation (Supplementary Figure 1).

To confirm that control and SZ hiPSC NPCs were comparably patterned, we specifically compared expression of 74 well-accepted markers of neural subtype identity in control and SZ NPCs and neurons (Supplementary Figure 2 and Supplementary Table 2). Of the 15/74 genes with perturbed expression, only four (*NEUROD1, MATH3, HOXB9* and *FOXO1*) were transcription factors, and of the others, six were synaptic genes, one was the extracellular matrix gene *RELN*, and three were enzymes involved in the synthesis of gamma-aminobutyric acid or dopamine (Supplementary Figure 2 and Supplementary Table 2).

When considering multiple markers of spatial and temporal identity, hiPSC NPCs show considerable inter-cell heterogeneity. Across SZ patients and controls, most hiPSC NPCs are positive for the NPC markers NESTIN (NES) and SOX2 (Supplementary Figure 3A). βIII-tubulin staining is visible in all NPC populations but does not appear to vary between control and SZ (Supplementary Figure 3A). Markers of neural stem cells, such as VIMENTIN (VIM) and PAX6, and neuronal progenitors, such as TBR2, are expressed by control and SZ hiPSC NPCs (Supplementary Figure 3A). There was no detectable difference in the labeling of control and SZ hiPSC NPCs by the cell cycle marker Ki67 (Supplementary Figures 3A and B). Doubling time between control hiPSC forebrain NPCs (3.69 ± 0.05 days) and SZ hiPSC forebrain NPCs (3.60 ± 0.02 days) did not differ ($P>0.5$) (Supplementary Figure 3C). Similarly, using cell cycle analysis, the percentage of cells in G1 ($62.3 \pm 0.2\%$ and $61.0 \pm 0.1\%$, $P>0.3$), S (24.6 ± 0.1 and 24.9 ± 0.1, $P>0.7$) and G2 (6.5 ± 0.03 and $6.5 \pm 0.02\%$, $P>0.3$) phases did not differ between control and SZ hiPSC forebrain NPCs (Supplementary Figure 3D). Regional patterning between NPC lines appears to be very similar, and NPC populations derived from control or SZ hiPSC NPCs lines do not appear to be either more proliferative or more neuronal. Although inter-NPC line differences in staining for these cortical neural stem cell and immature neurons markers did occur, hiPSC NPCs did not appear to vary by diagnosis.

Network analysis of gene expression of control and SZ hiPSC NPCs identifies perturbations in neuronal maturation and cellular adhesion

In all, 481 unique genes (134 upregulated and 347 downregulated) showed >1.30-fold expression changes between SZ and control hiPSC NPCs ($P < 0.05$) after correcting for multiple comparisons (Supplementary Figures 4A and B; Supplementary Table 3). The SZ hiPSC NPC gene signature (GS) overlapped significantly (Bonferroni-corrected, $P = 2.4e{-}30$, 4.9-fold) with our previously published SZ iPSC 6-week-old neuron GS,[11] and the consistency of the directions of the differential expressions in SZ hiPSC NPC GS and SZ hiPSC 6-week-old neuron GS was more significant than the inconsistency. For example, the up- and downregulated gene sets in SZ hiPSC NPC GS highly overlapped their counterparts in SZ hiPSC 6-week-old neuron GS (Bonferroni-corrected, $P < 1.8e{-}10$ (6.8-fold) and $1.6e{-}19$ (8-fold), respectively), whereas the up- and downregulated gene sets in SZ hiPSC NPC GS were very insignificantly enriched in the down- and upregulated gene sets in SZ hiPSC 6-week-old neuron GS (Bonferroni-corrected, $P = 0.4$ and 1, respectively). Much of the SZ 6-week-old neuron GS is conserved in SZ NPCs, suggesting that the molecular events contributing to SZ are established before neuronal differentiation.

We used WGCNA to identify modules composed of highly co-expressed genes[12] and found five gene modules (Figure 1b). Many of the gene modules identified in SZ hiPSC NPC GS predicted neuronal deficits (neuron differentiation, neuronal migration, glutamate receptor signaling and synaptic vesicle function), suggesting that neural deficits in SZ might be specified before neural differentiation. We validated 8/12 neuronal migration-associated candidate genes by qPCR across an increased number of individuals (six controls and four SZ patients) and NPC lines (two NPC lines per SZ patient; $\geqslant 1.3$-fold changes in expression; $P < 0.01$) (Figure 1c and Supplementary Table 4). We performed gene ontology analysis using manually curated databases; in addition to neurophysiological pathways involving synapse formation and synaptic transmission, our analysis also identified significant perturbations of cellular adhesion genes, (Supplementary Figures 4A and B, and 5D).

To assess the relevance of the SZ hiPSC NPC GS to the developing brain, it was compared with gene co-expression networks constructed based on the mRNA expression data from 16 cortical and subcortical structures across the full course of human brain development, including fetal and early childhood postmortem brain tissue (BrainSpan Atlas, http://www.brainspan.org/). The hiPSC NPC GS is most significantly enriched in the co-expressed gene modules from hippocampus (cell cycle module, $P = 5.7e{-}17$, 2.2-fold enrichment), medial prefrontal cortex (cell cycle module, $P = 5.9e{-}14$, 2.4-fold enrichment; synaptic transmission module, $P = 4.5e{-}8$, 2.9-fold enrichment), posterior superior temporal cortex (synaptic transmission module, $P = 3.5e{-}14$, 3.7-fold enrichment), inferolateral temporal cortex (neuropeptide signaling module, $P = 3e{-}11$, 3.6-fold enrichment), and striatum networks (synaptic transmission module, $P = 5.3e{-}11$, 2.1-fold enrichment). Interestingly, the upregulated genes in the hiPSC NPC GS are far more significantly enriched in these brain region-specific networks than the downregulated genes.

Proteomic analysis of control and SZ hiPSC NPCs identifies perturbations in cellular adhesion and oxidative stress pathways

Large-scale proteomic methods can identify quantitative differences in proteome-wide protein levels between control and diseased neural cells.[14] In Figure 2, we show that pairwise SILAC (stable isotope labeling by amino acids in cell culture) comparisons of control and SZ hiPSC NPCs identified changes in cellular adhesion and oxidative stress pathways. SILAC (Supplementary Figure 5A), in conjunction with multidimensional protein

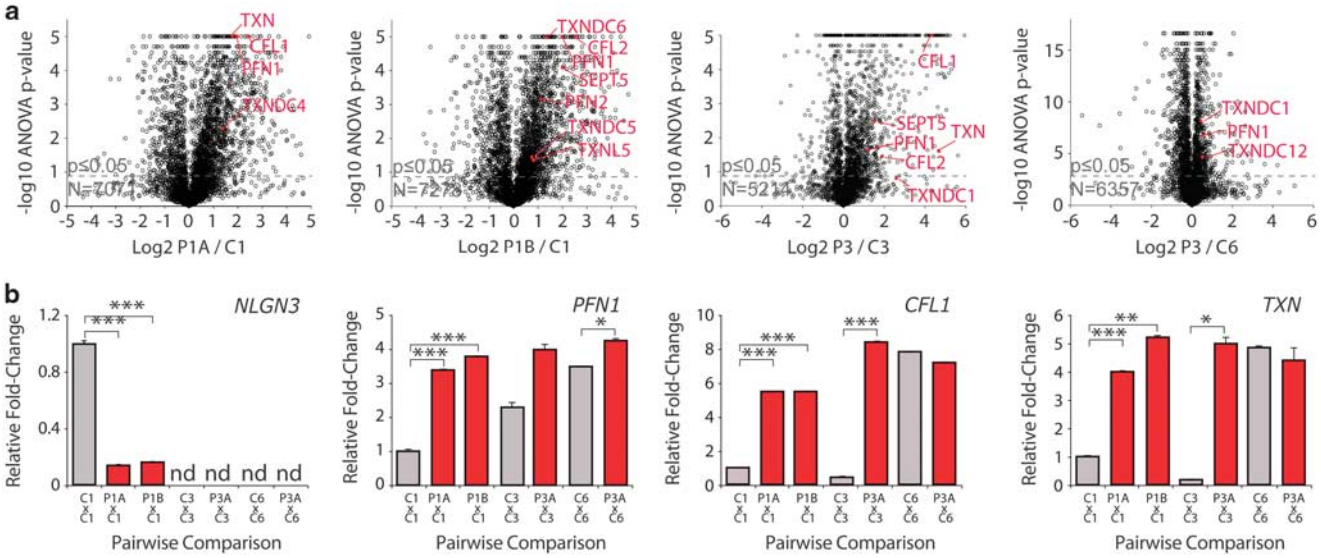

Figure 2. Aberrant expression of cytoskeletal and oxidative stress proteins in four independent pairwise SILAC (stable isotope labeling by amino acids in cell culture) quantitative proteomic mass spectrometry comparisons of control and schizophrenia (SZ) human induced pluripotent stem cell (hiPSC) forebrain neural progenitor cells (NPCs). (**a**) Volcano plots of −log10 analysis of variance *P*-value versus log2 SZ/control protein levels for pairwise analyses of NPCs from patient 1 (left) and patient 3 (right) compared with gender-matched controls 1, 3 or 6, respectively. Key cytoskeletal remodeling proteins (cofilins and profilins) and oxidative stress proteins (thioredoxin and related proteins) are highlighted. From left to right, $N = 7072$, 7226, 5215 and 6357 proteins. (**b**) Bar graphs showing decreased NLGN3 in P1 SILAC comparisons and increased PFN1, CFL1 and TXN protein levels in four independent SILAC comparisons. Error bars are s.e.m., $^{*}P < 0.05$, $^{**}P < 0.01$, $^{***}P < 0.001$. See also Supplementary Figure 5.

identification technology, was used to identify proteins that were up- or downregulated in four pairwise comparisons (consisting of 5 'heavy' and 5 'light' quantitative mass spectrometry analysis runs per cell line) between gender-matched SZ (P1 and P3) and control (C1, C3 and C6) hiPSC NPCs. Although labeling efficiency was high (Supplementary Figure 5C), ratio-of-ratios analysis (control-heavy/SZ light relative to control-heavy/control light) permitted correction of any incompletely labeled proteins by the fractional analysis. When the same 74 markers of neural subtype identity used to compare microarray gene expression profiles were considered across our four SILAC protein data sets, only one (NCAM1) was significantly perturbed in both patients analyzed (Supplementary Table 2). Through four independent SILAC experiments, we identified perturbed proteins with corrected *P*-values < 0.05 and >1.2-fold change in SZ hiPSC NPCs (Supplementary Tables 5–8). These data are illustrated in volcano plots representing relative protein levels in our four independent pairwise comparisons: key cytoskeletal remodeling proteins(cofilins (CFL1 and CFL2) and profilins (PFN1 and PFN2)) and oxidative stress proteins (thioredoxin (TXN) and related proteins) have been highlighted (Figure 2a).

Many of the most perturbed proteins identified in P1 NPC line A (relative to C1 NPC) were similarly affected in an independent SILAC in comparison with P1 NPC line B (relative to C1 NPC); for example, a known SZ protein, NLGN3, was significantly downregulated in both P1 NPCA and P1 NPC B (Figure 2b). When we subsequently compared a second SZ patient (P3 NPC) with a second and third control (C3 and C6 NPC), we observed several notable changes across independent pairwise comparisons. Three actin-binding proteins involved in cytoskeletal restructuring and migration, profilin (PFN1) and two cofilins (CFL1 and CFL2), were significantly upregulated in SZ in at least three comparisons (Figure 2b). In addition, TXN was significantly upregulated in SZ in three comparisons (Figure 2b) (and many related proteins such as TXNL1, TXNL2, TXNDC1, TXNDC4, TXNDC5, TXNDC12 and TXNRD1 were also upregulated in one or more comparisons; Supplementary Tables 5–8). The high degree of similarity between the four pairwise SILAC analyses (Figure 2; Supplementary Tables 5–8) is clearly evident by gene ontology analysis, which identified oxidative stress/apoptosis and cytoskeletal remodeling pathways in all comparisons (Supplementary Figure 5D). Increased PFN1 (14 kDa) protein was subsequently validated across six controls and four patients by western blot, relative to an actin loading control (Supplementary Figure 5B).

Aberrant cell migration in SZ hiPSC NPCs

Through three independent assays presented in Figure 3—neurosphere migration, microfluidic device migration and laminin spot 'chaining'—we observed aberrant migration in SZ hiPSC NPCs. Neurosphere outgrowth is an established assay whereby the distance that NPCs migrate from a neurosphere is measured. We compared outgrowth from 241 control and 324 SZ neurospheres, generated by culturing NPCs in non-adherent conditions for 72 h and then plating them in three-dimensional Matrigel conditions, in a method similar to one previously developed for embryonic stem cell-derived neurospheres.[15] There was significantly reduced outgrowth from SZ neurospheres (269 ± 6 μm) relative to controls (368 ± 5 μm; $P < 0.00001$), in conditions supporting either proliferation or neural differentiation (Figures 3a and b; Supplementary Figures 6A and B). Culture of SZ neurospheres with media conditioned by control hiPSC NPCs, and culture of control neurospheres with media conditioned by SZ hiPSC NPCs did not affect migration (672 neurospheres analyzed; Figure 3c). Neither mixing control and SZ hiPSC NPCs (marked through reciprocal labeling of lentiviral green fluorescent protein or red fluorescent protein expression) before neurosphere migration (288 neurospheres analyzed; Figures 3d and e) nor culturing lentiviral-green fluorescent protein-labeled neurospheres on healthy cortical murine tissue in slice coculture conditions (147 neurospheres analyzed; Supplementary Figures 6C and D) rescued aberrant migration of SZ NPCs, indicating that this may be a cell-autonomous defect. Using microfluidic devices to probe the

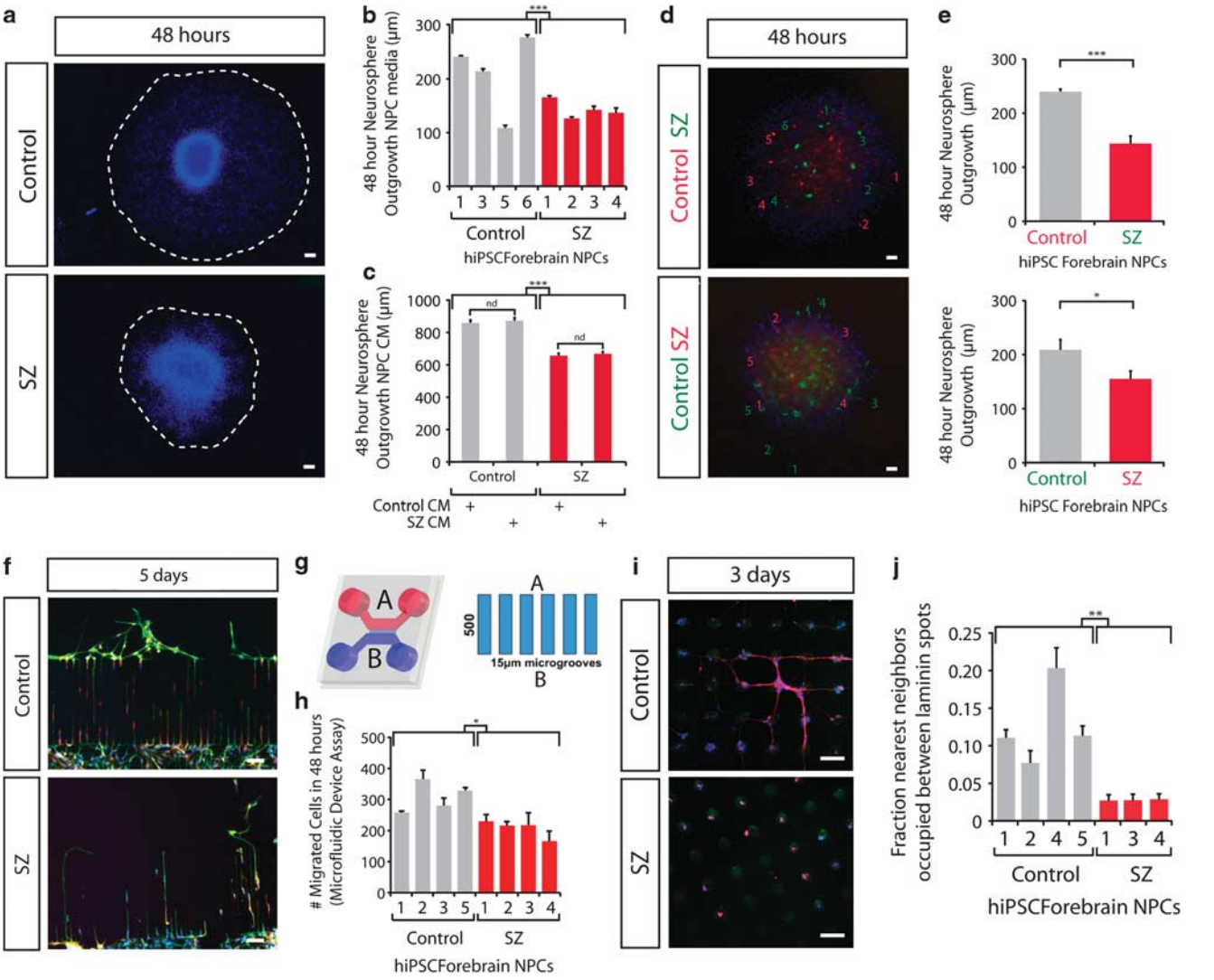

Figure 3. Aberrant migration in schizophrenia (SZ) human-induced pluripotent stem cell (hiPSC) forebrain neural progenitor cells (NPCs). (**a**) Representative images of hiPSC forebrain NPC neurosphere outgrowth assay. The average distance between the radius of the inner neurosphere (dense aggregate of nuclei) and outer circumference of cells (white dashed line) was calculated. 4′,6-Diamidino-2-phenylindole (DAPI)-stained nuclei (blue). Scale bar, 100 μm. (**b**) Neurosphere outgrowth by control and SZ hiPSC forebrain NPCs. (**c**) Neurosphere outgrowth following coculture with control or SZ hiPSC NPC-conditioned media (CM). (**d**) Representative images of mixed control and SZ hiPSC NPCs, labeled with lentivirus-green fluorescent protein and lentivirus-red fluorescent protein. Green and red numbers indicate five furthest migrated lentiviral-green fluorescent protein and lentiviral-red fluorescent protein NPCs in reciprocal migration experiments. DAPI-stained nuclei (blue). Scale bar 100 μm. (**e**) Neurosphere outgrowth in neurospheres composed of mixed control and SZ hiPSC NPCs. (**f**) Representative images of hiPSC forebrain NPCs after 5 days in a microfluidic device. At time 0, all NPCs were below the microgrooves pictured—migration occurred up from chamber B into chamber A. Migrating neural cells stained with MAP2AB (red), βIII-tubulin (green); DAPI-stained nuclei (blue). Scale bar, 100 μm. (**g**) Schematic of the microfluidic chambers. At time 0, hiPSC NPCs were added to chamber B and allowed to begin migration toward chamber A via 15-μm grooves. (**h**) Cellular migration of control and SZ hiPSC NPCs in microfluidic devices at 48 h. (**i**) Representative images of hiPSC forebrain NPCs in micropatterned laminin spot migration assay. Laminin spot stained (green); migrating neural cells stained with βIII-tubulin (red); and DAPI-stained nuclei (blue). Scale bar, 100 μm. (**j**) Nearest-neighbor analysis of 'chaining' between laminin spots by control and SZ hiPSC forebrain NPCs. Error bars are s.e.m., $^{*}P < 0.05$, $^{**}P < 0.01$, $^{***}P < 0.001$. See also Supplementary Figures 6–8.

migration of single cells, with NPCs from five controls and four patients, we observed reduced migration of SZ hiPSC forebrain NPCs (207 ± 6 migrated cells after 48 h) relative to controls (277 ± 5 migrated cells; $P < 0.02$) (Figures 3f–h). Finally, when migration across discrete micropatterned laminin spots coated on a gold-plated hydrophobic biomaterials surface was assessed, we observed a markedly decreased percentage of neurosphere 'chaining' between laminin spots in SZ hiPSC forebrain NPCs (SZ 2.8 ± 0.3%) relative to controls (12.8 ± 0.5%; $P < 0.0005$) (Figures 3i and j). Reduced migration is unlikely to reflect impaired cellular motility; although we report decreased migration in SZ with three assays (Figure 3), we observed significantly increased migration using a scratch assay (Supplementary Figure 7).

Immunohistochemical characterization revealed that hiPSC NPCs undergo rapid differentiation during the course of our migration assays. Although migrating cells are frequently βIII-tubulin-positive at the end point of these experiments, NES-positive cells are also capable of migration in all three assays (Supplementary Figure 8). Our migration assays appear to facilitate migration concurrent with neuronal differentiation.

While our SILAC data identified upregulation of the actin-binding proteins (PFN1, CFL1 and CFL2), which are direct targets

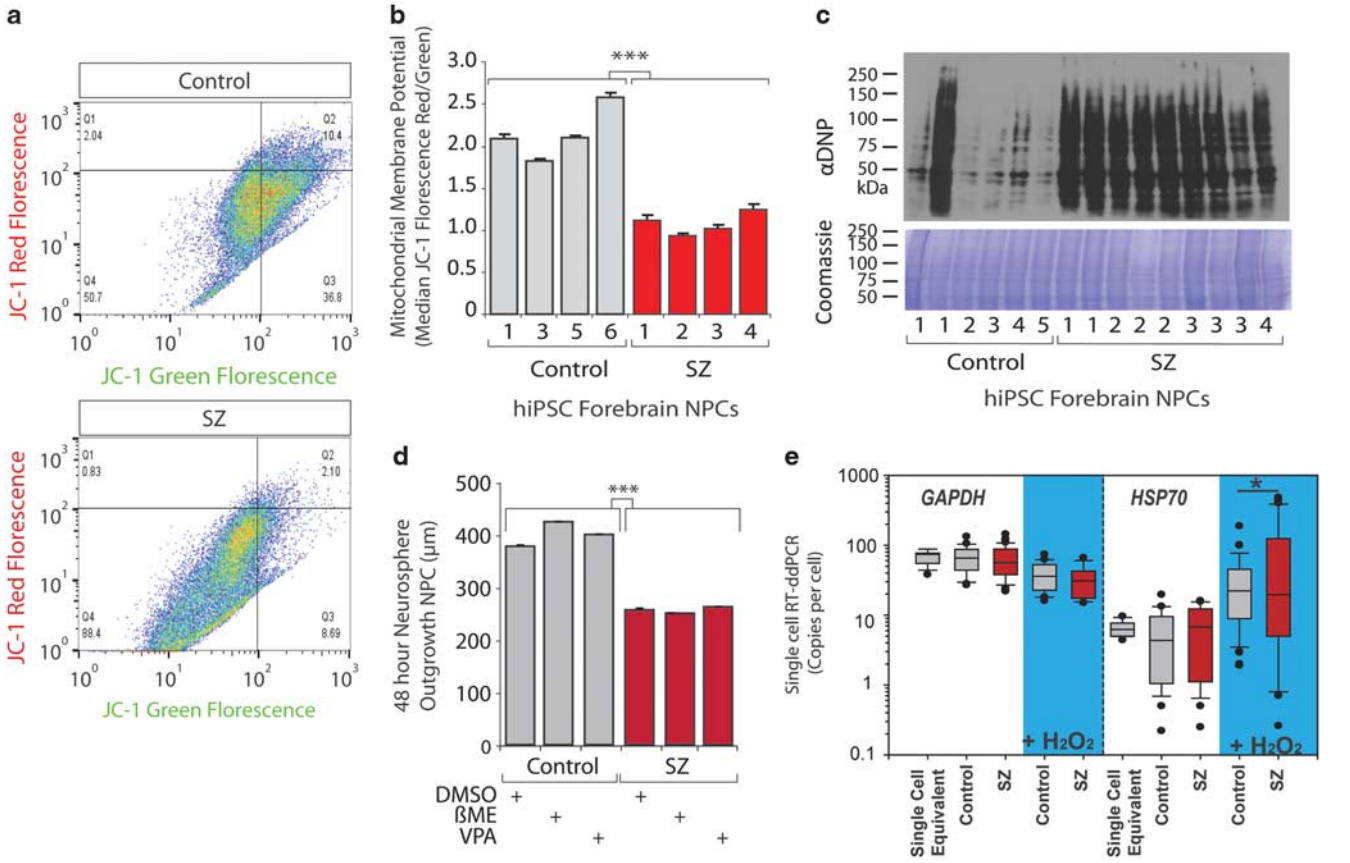

Figure 4. Mitochondrial damage and increased oxidative stress in schizophrenia (SZ) human-induced pluripotent stem cell (hiPSC) neural progenitor cells (NPCs). (**a**) Representative fluorescence-activated cell sorting (FACS) plots for JC-1 red/green fluorescence in control and SZ hiPSC NPCs. (**b**) FACS analysis for mitochondrial membrane potential (MMP) in control and SZ hiPSC NPCs indicated by median JC-1 red/green fluorescence. (**c**) OxyBlot western blot for oxidized proteins in SZ hiPSC NPCs. (**d**) Neurosphere outgrowth by control and SZ hiPSC forebrain NPCs with and without treatment by the anti-oxidant β-mercaptoethanol or valproic acid (VPA). (**e**) Graph shows fold change of *GAPDH* and *HSP70* expression following H_2O_2 treatment compared with PBS exposure. There was significantly increased variability observed in SZ hiPSC NPCs as compared with the control ($n>50$), but no significant differences in the means in all sets of comparisons. Error bars are s.e.m., $^*P < 0.05$, $^{***}P < 0.001$. See also Supplementary Figure 9.

of RHO/ROCK activity, the ROCK inhibitor Y27632 failed to ameliorate aberrant SZ migration, instead significantly inhibiting migration of both control ($P < 0.00001$) and SZ ($P < 0.000001$) neurospheres (128 total SZ neurospheres were analyzed relative to 112 total control neurospheres) (Supplementary Figure 6I).

Antipsychotic manipulation of aberrant SZ hiPSC NPC migration

We tested the ability of the clinical antipsychotics to rescue SZ neurosphere migration: treatment with neither loxapine nor clozapine improved aberrant migration of SZ neurospheres (463 total SZ neurospheres were analyzed relative to 428 total control neurospheres). Clozapine had no significant effect on SZ neurosphere migration in this assay (Supplementary Figure 6F). Forty-eight-hour loxapine treatment reduced migration of control ($P < 0.007$) and SZ neurospheres ($P < 0.02$), an effect that was substantially exaggerated following 7 days of loxapine treatment ($P < 0.0001$; Supplementary Figures 6F and G). This loxapine-induced reduced neurosphere migration cannot be attributed to decreased cellular replication of NPCs, as assayed immunohistochemically by staining for the cell cycle marker Ki67 (Supplementary Figure 6H). Nanostring gene expression comparisons of loxapine-treated and loxapine-untreated NPCs found decreased expression of many neuronal adhesion genes, particularly *NCAM1*, *NRG3, NLGN1 and NLGN2*, following 7 days of loxapine treatment (Supplementary Figure 6J).

Mitochondrial damage and increased oxidative stress observed in SZ hiPSC NPCs

In Figure 4, we demonstrate mitochondrial damage and increased oxidative stress in SZ hiPSC NPCs. MMP ($\Delta\Psi m$) is the voltage difference across the inner mitochondrial membrane. MMP and cytosolic reactive oxidative stress (ROS) are intricately and inversely related: increased ROS can decrease MMP through various mechanisms, whereas mitochondrial dysfunction (decreased MMP) can increase ROS.[16] We assayed MMP using JC-1 lipophilic cationic dye. The fluorescence of JC-1 dye changes from green to red as MMP increases, an inverse measure of oxidative stress (Figure 4a). We observed significantly decreased MMP (median intensity of JC-1 red/green fluorescence), indicative of increased oxidative stress, in SZ hiPSC NPCs (2.20 ± 0.07) relative to control hiPSC NPCs (1.09 ± 0.03) ($P < 0.00001$; Figure 4a and b). Immunohistochemical staining for the mitochondrial marker MTC02 revealed that mitochondria in SZ hiPSC NPCs tended to be smaller, disconnected and distally distributed, whereas mitochondria in control hiPSC NPCs tended to be more connected, tubular and highly packed near the perinuclear regions (Supplementary Figure 9A). Exceptions were that some mitochondria from Patient 3 were connected and/or

packed, whereas some from patient 4 were tubular (Supplementary Figure 9A). Transmission electron microscopic analysis confirmed these features (Supplementary Figure 9B).

In conditions of ROS, the oxidative modification of proteins introduces carbonyl groups (aldehydes and ketones) at Lys, Arg, Pro or Thr amino-acid residues. An OxyBlot assay revealed more ROS-induced oxidized proteins in the SZ hiPSC NPCs (Figure 4c).

Cell death enzyme-linked immunosorbent assay, a photometric enzyme immunoassay for cytoplasmic histone-associated DNA fragments associated with apoptosis, detected increased DNA fragmentation consistent with apoptosis in SZ NPCs (1.446 ± 0.003) relative to controls (1.18 ± 0.05; $P < 0.001$) (Supplementary Figure 3E). A cytotoxicity assay that indirectly measures the lactate dehydrogenase activity present in the cytoplasm of the intact cells did not detect differences between control (19.6 ± 2.1) and SZ (17.1 ± 0.7) NPCs ($P>0.19$) (Supplementary Figure 3F). By most, but not all measures, increased oxidative stress did not appear to meaningfully affect survival (Supplementary Figures 3E and F) and/or replication (Supplementary Figure 3B, C and D) of SZ hiPSC NPCs under routine culture conditions.

Culture with neither the reducing agent β-mercaptoethanol nor the mood stabilizer valproic acid, which was previously reported to reduce increased extra-mitochondrial oxygen consumption in SZ hiPSC neural cells,[17] was capable of ameliorating aberrant migration of SZ neurospheres (264 total SZ neurospheres were analyzed relative to 262 total control neurospheres; $P>0.7$) (Figure 4d).

Increased cell-to-cell variation in stress response among SZ hiPSC NPCs. A number of prenatal environmental risk factors have been reported to potentially contribute to SZ,[18] and abnormalities in HSF1-HSP70 signaling have been linked to SZ.[19,20] Two independent NPC lines from each of four patients with SZ were given sub-threshold environmental challenges of oxidative stress (0.05 mM H_2O_2) for 3 h. Following treatment, we measured the expression of *HSP70* and *GAPDH* in individual NPCs; all NPC lines showed increased *HSP70* expression in response to challenge (Figure 4e). Notably, although average change of *HSP70* expression did not differ between control and SZ hiPSC NPCs, cell-to-cell variability in *HSP70* expression was significantly larger in SZ hiPSC NPCs following sub-threshold oxidative stress (Figure 4e). We did not observe any difference in cell-to-cell variability in *GAPDH* measurements, and there was no significant correlation ($P = 0.22$) between the expression levels of *GAPDH* and *HSP70*, suggesting that cell-to-cell variability was specific to *HSP70* expression. Single-cell equivalents, generated by pooling the lyses of 10 cells and aliquoting 1/10th to use as a single-cell equivalent, showed very small variability (Figure 4e). Stress response, as mediated by *HSF1*, may be abnormal in a subpopulation of SZ hiPSC NPCs at the single-cell level.

DISCUSSION

From gene expression in comparisons with the Allen BrainSpan Atlas, we demonstrate that hiPSC forebrain NPCs and 6-week-old neurons more closely resemble fetal brain tissue. Although our extensive characterization of spatial and temporal identity revealed that hiPSC NPCs show inter-cell and inter-line heterogeneity, variation between hiPSC NPCs lines does not explain the consistent SZ-associated hiPSC NPC phenotypes observed. Using two unbiased discovery-based approaches, microarray gene expression and SILAC quantitative proteomic mass spectrometry, we predicted, and observed, aberrant migration and increased oxidative stress in a pilot cohort of SZ hiPSC NPCs, although effect sizes were insufficient to predict diagnosis. We are the first to report aberrant migration in SZ hiPSC neural cells, and we have doubled the number of SZ patients from which hiPSC neural cells show increased oxidative stress.[17,21] We conclude that gene expression and proteomic data sets can be used to identify novel cellular phenotypes of SZ, but we caution that, because of our small sample size, these phenotypes may not generalize across all SZ patients.

When Gulsuner *et al.*[4] mapped the 57 damaging *de novo* mutations they identified in persons with SZ onto transcriptome profiles of normal human brain tissues, they found that, specifically in the fetal prefrontal cortex, affected genes formed a network that functioned in neuronal migration, synaptic transmission and transcriptional regulation. These results suggest that disruptions of fetal prefrontal cortical neurogenesis are critical to the pathophysiology of SZ; consistent with this, abnormalities of cortical neuronal organization in postmortem SZ brains[22] have been reported. Aberrant migration[23] and distribution[24] of interneurons, reduced neurite outgrowth[25,26] and abnormal axon targeting[27] occur in mouse models of SZ.

In the developing cortex, most migrating neural cells are post mitotic. In our experiments, neuronal differentiation is rapidly initiated, and both NES-positive and βIII-tubulin-positive migrating neural cells can be detected. Our observations do not necessarily imply that abnormal *in utero* neural migration leads to SZ. Although increased SZ hiPSC NPC migration in the scratch assay seems inconsistent with our observation of decreased migration across three neural migration assays, scratch assays more accurately model wound healing rather than neural migration, implying that the defect in SZ hiPSC NPCs lies not in motility but in cellular adhesion. Many of the cellular migration genes decreased in SZ hiPSC NPCs, including NCAM, NRXNs and NLGNs, are also required for synaptic adhesion; aberrant migration of SZ hiPSC NPCs may arise from the very same mechanisms leading to decreased neuronal connectivity in SZ neurons. The further perturbation, rather than amelioration, of SZ neurosphere migration by the antipsychotic loxapine suggests that the relationship between synaptic function and migration is not straightforward.

Elevated oxidative stress and extra-mitochondrial oxygen consumption are also speculated to contribute to SZ.[28] Cell-to-cell variability in transcription has been well recognized in microbial cells, particularly in cellular stress-responsive genes,[29] and elevated cell-to-cell transcriptional variability in aged cardiomyocytes occurs as a result of increased genome damage by oxidative injury.[30] The mechanisms producing higher variability in the HSF1 activation in SZ hiPSC NPCs requires further investigation.

The limited overlap of our gene expression and protein data sets warrants discussion. Cellular RNA and protein levels are imperfectly associated, with a correlation coefficent < 0.7,[31] likely owing to a combination of post-transcriptional effects, rapid translation and protein turnover. In addition, our SILAC methods were unlikely to detect secreted proteins, such as RELN and other extracellular matrix proteins, that were significantly perturbed in our microarrays. In fact, of the 483 significantly misexpressed genes identified by microarray analysis, most were poorly detected as proteins by mass spectrometry (Supplementary Table 9). Of those significantly misexpressed genes detected and identified as significantly perturbed in three of our four SILAC mass spectrometry analyses, there was an enrichment in the predicted direction of change (binomial test *P*-values: 5.6053e–04, 3.9675e–05, 0.1442, 2.0013e–09), while there was no effect in the opposite direction. Our gene and protein data sets were more consistent at the pathway level (Supplementary Figure 5D).

SZ hiPSC NPCs revealed reproducible SZ-associated phenotypes; future studies must now demonstrate they relate to disease etiology. SZ hiPSC NPCs may serve as a proxy for the developmental pathways potentially contributing to SZ pathogenesis, much as Huntington's disease hiPSC NPCs have been shown to recapitulate elements of Huntington's disease pathogenesis.[32] *In vitro* assays for neural migration and oxidative stress are scalable and amenable to high-throughput screening. This approach is suitable for large cohorts of SZ patients, making it a potentially valuable tool in the study of this complex and heterogeneous disorder.

CONFLICT OF INTEREST

The authors declare no conflict of interest.

ACKNOWLEDGMENTS

L Moore, B Miller, K Stecker, A Patruno, J Rose, E Xia and S Larkin provided technical assistance. The Salk Stem Cell facility, the Salk Viral Vector Core and the Icahn School of Medicine Stem Cell Core all provided support. J Nguyen and L Ouyang provided gene expression support. D Chambers provided FACS support, ML Gage provided editorial comments. We thank M McConnell, C Marchetto and L Boyer for their advice and conversation. The Gage Laboratory is partially funded by California Institute of Regenerative Medicine (CIRM) grant RL1-00649-1, the G Harold & Leila Y Mathers Foundation, the JPB Foundation, the Leona M and Harry B Helmsley Charitable Trust, Annette Merle-Smith, and Robert and Mary Jane Engman. Kristen Brennand is a New York Stem Cell Foundation—Robertson Investigator. The Brennand Laboratory is supported by a Brain and Behavior Young Investigator Grant, National Institute of Health (NIH) grant R01 MH101454 and the New York Stem Cell Foundation. The Yates laboratory is supported by NIH grants R01 MH068770, P41 GM103533 and R01MH100175, while JNS is supported by National Research Service Award (NRSA) fellowship F32 AG039127 and F Hoffman-La Roche Postdoctoral Fellowship Award SFP2063. The Rakic laboratory is supported by NIH grants R01 DA023999 and R01 NS014841, and the Kavli Institute for Neuroscience at Yale. The Hashimoto-Torii laboratory is funded by NARSAD, CTSI-CN and R00 AA018387. The Zhang laboratory is supported by R01 AG046170, R21 MH097156-01A1, R01 CA163772 and U01AI111598-01. The Mrksich laboratory is funded by the Chicago Biomedical Consortium with support from the Searle Funds at The Chicago Community Trust.

AUTHOR CONTRIBUTIONS

KJB and FHG designed the experiments and wrote the manuscript. Experiments were completed and analyzed as follows: SILAC quantitative proteomic experiments (JNS and JRY), oxidative stress and mitochondrial damage experiments (YK), migration experiments (NT assisted by BM-A, MA and IL), microarray and qPCR experiments (AS), western blots (AT), single-cell stress assay (KH-T and PR, and S-hC designed the MOCCA single-cell separation), micropatterned laminin spot migration assay (KGB and MM), microfluidic device migration assays (HJK). Computational analysis was completed by GF and BZ.

REFERENCES

1 Weinberger DR. Implications of normal brain development for the pathogenesis of schizophrenia. *Arch Gen Psychiatry* 1987; **44**: 660–669.
2 White T, Anjum A, Schulz SC. The schizophrenia prodrome. *Am J Psychiatry* 2006; **163**: 376–380.
3 Wong AH, Van Tol HH. Schizophrenia: from phenomenology to neurobiology. *Neurosci Biobehav Rev* 2003; **27**: 269–306.
4 Gulsuner S, Walsh T, Watts AC, Lee MK, Thornton AM, Casadei S *et al.* Spatial and temporal mapping of *de novo* mutations in schizophrenia to a fetal prefrontal cortical network. *Cell* 2013; **154**: 518–529.
5 Nicholas CR, Chen J, Tang Y, Southwell DG, Chalmers N, Vogt D *et al.* Functional maturation of hPSC-derived forebrain interneurons requires an extended timeline and mimics human neural development. *Cell Stem Cell* 2013; **12**: 573–586.
6 Mariani J, Simonini MV, Palejev D, Tomasini L, Coppola G, Szekely AM *et al.* Modeling human cortical development *in vitro* using induced pluripotent stem cells. *Proc Natl Acad Sci USA* 2012; **109**: 12770–12775.
7 Espuny-Camacho I, Michelsen KA, Gall D, Linaro D, Hasche A, Bonnefont J *et al.* Pyramidal neurons derived from human pluripotent stem cells integrate efficiently into mouse brain circuits *in vivo*. *Neuron* 2013; **77**: 440–456.
8 Maroof AM, Keros S, Tyson JA, Ying SW, Ganat YM, Merkle FT *et al.* Directed differentiation and functional maturation of cortical interneurons from human embryonic stem cells. *Cell Stem Cell* 2013; **12**: 559–572.
9 Hu BY, Du ZW, Zhang SC. Differentiation of human oligodendrocytes from pluripotent stem cells. *Nat Protoc* 2009; **4**: 1614–1622.
10 Wang S, Bates J, Li X, Schanz S, Chandler-Militello D, Levine C *et al.* Human iPSC-derived oligodendrocyte progenitor cells can myelinate and rescue a mouse model of congenital hypomyelination. *Cell Stem Cell* 2013; **12**: 252–264.
11 Brennand KJ, Simone A, Jou J, Gelboin-Burkhart C, Tran N, Sangar S *et al.* Modelling schizophrenia using human induced pluripotent stem cells. *Nature* 2011; **473**: 221–225.
12 Wang IM, Zhang B, Yang X, Zhu J, Stepaniants S, Zhang C *et al.* Systems analysis of eleven rodent disease models reveals an inflammatome signature and key drivers. *Mol Syst Biol* 2012; **8**: 594.
13 Butko MT, Savas JN, Friedman B, Delahunty C, Ebner F, Yates JR3rd *et al. In vivo* quantitative proteomics of somatosensory cortical synapses shows which protein levels are modulated by sensory deprivation. *Proc Natl Acad Sci USA* 2013; **110**: E726–E735.
14 Liao L, Park SK, Xu T, Vanderklish P, Yates JR 3rd. Quantitative proteomic analysis of primary neurons reveals diverse changes in synaptic protein content in fmr1 knockout mice. *Proc Natl Acad Sci USA* 2008; **105**: 15281–15286.
15 Delaloy C, Liu L, Lee JA, Su H, Shen F, Yang GY *et al.* MicroRNA-9 coordinates proliferation and migration of human embryonic stem cell-derived neural progenitors. *Cell Stem Cell* 2010; **6**: 323–335.
16 Satoh T, Enokido Y, Aoshima H, Uchiyama Y, Hatanaka H. Changes in mitochondrial membrane potential during oxidative stress-induced apoptosis in PC12 cells. *J Neurosci Res* 1997; **50**: 413–420.
17 Paulsen BD, de Moraes Maciel R, Galina A, Souza da Silveira M, dos Santos Souza C, Drummond H *et al.* Altered oxygen metabolism associated to neurogenesis of induced pluripotent stem cells derived from a schizophrenic patient. *Cell Transplant* 2012; **21**: 1547–1559.
18 Sullivan PF. The genetics of schizophrenia. *PLoS Med* 2005; **2**: e212.
19 Kim JJ, Lee SJ, Toh KY, Lee CU, Lee C, Paik IH. Identification of antibodies to heat shock proteins 90 kDa and 70 kDa in patients with schizophrenia. *Schizophr Res* 2007; **52**: 127–135.
20 Pae CU, Kim TS, Kwon OJ, Artioli P, Serretti A, Lee CU *et al.* Polymorphisms of heat shock protein 70 gene (HSPA1A, HSPA1B and HSPA1L) and schizophrenia. *Neurosci Res* 2005; **53**: 8–13.
21 Robicsek O, Karry R, Petit I, Salman-Kesner N, Müller FJ, Klein E *et al.* Abnormal neuronal differentiation and mitochondrial dysfunction in hair follicle-derived induced pluripotent stem cells of schizophrenia patients. *Mol Psychiatry* 2013; **18**: 1067–1076.
22 Akbarian S, Kim JJ, Potkin SG, Hetrick WP, Bunney WEJr, Jones EG. Maldistribution of interstitial neurons in prefrontal white matter of the brains of schizophrenic patients. *Arch Gen Psychiatry* 1996; **53**: 425–436.
23 Meechan DW, Tucker ES, Maynard TM, LaMantia AS. Cxcr4 regulation of interneuron migration is disrupted in 22q11.2 deletion syndrome. *Proc Natl Acad Sci USA* 2012; **109**: 18601–18606.
24 Meechan DW, Tucker ES, Maynard TM, LaMantia AS. Diminished dosage of 22q11 genes disrupts neurogenesis and cortical development in a mouse model of 22q11 deletion/DiGeorge syndrome. *Proc Natl Acad Sci USA* 2009; **106**: 16434–16445.
25 Kvajo M, McKellar H, Arguello PA, Drew LJ, Moore H, MacDermott AB *et al.* A mutation in mouse Disc1 that models a schizophrenia risk allele leads to specific alterations in neuronal architecture and cognition. *Proc Natl Acad Sci USA* 2008; **105**: 7076–7081.
26 Krivosheya D, Tapia L, Levinson JN, Huang K, Kang Y, Hines R *et al.* ErbB4-neuregulin signaling modulates synapse development and dendritic arborization through distinct mechanisms. *J Biol Chem* 2008; **283**: 32944–32956.
27 Faulkner RL, Jang MH, Liu XB, Duan X, Sailor KA, Kim JY *et al.* Development of hippocampal mossy fiber synaptic outputs by new neurons in the adult brain. *Proc Natl Acad Sci USA* 2008; **105**: 14157–14162.
28 Behrens MM, Sejnowski TJ. Does schizophrenia arise from oxidative dysregulation of parvalbumin-interneurons in the developing cortex? *Neuropharmacology* 2009; **57**: 193–200.
29 Avery SV. Microbial cell individuality and the underlying sources of heterogeneity. *Nat Rev Microbiol* 2006; **4**: 577–587.
30 Bahar R, Hartmann CH, Rodriguez KA, Denny AD, Busuttil RA, Dollé ME *et al.* Increased cell-to-cell variation in gene expression in ageing mouse heart. *Nature* 2006; **441**: 1011–1014.
31 Gry M, Rimini R, Strömberg S, Asplund A, Pontén F, Uhlén M *et al.* Correlations between RNA and protein expression profiles in 23 human cell lines. *BMC Genomics* 2009; **10**: 365.
32 An MC, Zhang N, Scott G, Montoro D, Wittkop T, Mooney S *et al.* Genetic correction of Huntington's Disease phenotypes in induced pluripotent stem cells. *Cell Stem Cell* 2012; **11**: 253–263.

Supplementary Information accompanies the paper on the Molecular Psychiatry website (http://www.nature.com/mp)